JOURNAL OF AIRCRAFT
Vol. 40, No. 2, March–April 2003

New Model of Decelerating Bluff-Body Drag

J. Potvin*
Saint Louis University, St. Louis, Missouri 63103
G. Peek†
Industrologic, Inc., St. Charles, Missouri 63301
and
B. Brocato‡
Saint Louis University, St. Louis, Missouri 63103

A new model of the drag force generated by a freely decelerating bluff body is presented. The model is based, mainly, on the premise that the wake of an object accelerating downwind in a moving fluid is identical to that of the same object decelerating in the fluid at rest. After arguing for the drag of a wind drifter to depend only on a power function of its speed relative to the wind, a Galilean transformation is used to provide a formula for decelerating body drag of the form $F_D \sim V^{\beta}$. The value of exponent β is dependent on the amount of external force applied to the body, as well as on its initial and final drag coefficients and its initial speed. By implication, this exponent depends on the specific history of the motion. Applications to powered and unpowered vehicles trailing a parachute or any other high-drag devices are presented and discussed. The model is also shown to compare favorably with parachute-test drop data.

Nomenclature

$a(t)$	=	instant acceleration or deceleration
b_0	=	initial value of the drag area used in Eq. (18)
b_1	=	time-normalized drag area difference used in Eq. (18)
C_D^{disk}	=	drag coefficient of a disk accelerating in a static fluid
C_D^{steady}	=	drag coefficient in steady motion
C^{init}	=	initial value of the drag function
$C(t)$	=	instant drag function; defined by Eq. (1)
D	=	characteristic diameter
F_D	=	force of drag
F_{ext}	=	external force
F_{tot}	=	net force applied on a moving body
K	=	constant used in Eq. (13)
S	=	reference surface area
T_{decel}	=	deceleration timescale
t_f^{infl}	=	ending time of the parachute inflation phase
V_f	=	speed at the end of an unsteady motion
V_i	=	speed at the beginning of an unsteady motion
V_{ref}	=	speed of a particular reference frame
V_{rel}	=	speed of a moving object relative to the incoming air/fluid
V_T	=	terminal speed, which arises from F_D balancing F_{ext} [Eq. (4)]
$V(t)$	=	instant speed of the body
β	=	exponent defined in Eq. (7)
δ	=	acceleration modulus; defined by Eq. (6)
δ_i	=	initial acceleration modulus
ε	=	time increment
v_{chute}	=	air volume contained inside a parachute and moving along with the parachute
v_{disk}	=	volume of a sphere featuring the same diameter as the disk located at its equator
ρ	=	air density

Superscript

$'$	=	quantities measured in an alternate Galilean reference frame

Received 6 July 2002; revision received 15 December 2002; accepted for publication 19 December 2002.

*Associate Professor, Department of Physics, Parks College Parachute Research Group; potvinj@slu.edu. Member AIAA.
†Consultant, Parks College Parachute Research Group, 3201 Highgate Lane, St. Charles, MO 63301; peek@industrologic.com.
‡Research Assistant, Parks College Parachute Research Group. Student Member AIAA.

Introduction

INFLATED parachutes and other high-drag objects often travel along trajectories that are far from being characterized by a constant velocity and constant drag coefficient.[1,2] During flight or cruise they may undergo unsteady motions such as during a turn maneuver, or during oscillations caused by accumulated excess air spilling from alternate sides.[3–16] Time-dependent speeds are of course seen during parachute inflation and also right after inflation when the fully inflated canopy then decelerates to the terminal velocity regime.[17–20] This means that, even at constant surface area, these objects may feature a ratio $F_D(t)/V(t)^2$ that is not only time dependent but also motion- and trajectory-dependent. In other words, defining the drag force of a moving body of constant surface area S through[21]

$$F_D(t) = \tfrac{1}{2}C(t)\rho S v(t)^2 \tag{1}$$

yields a time-dependent $C(t)$ (or drag function). This force coefficient is calculated solely from the independent measurements of S, $F_D(t)$, and $V(t)$, the latter usually being the speed of the body relative to the air/fluid at infinity. For example, Iversen and Balent report a drag function changing in the range of $0 < C(t) < 10$ in their tow tank study of accelerating disks.[22] Higuchi et al.,[23] Balligand and Higuchi,[24,25] and Strickland and Macha[26] also showed $C(t)$ to change by similar amounts for disks decelerating in a tow tank[23–25] and for freely decelerating high-speed porous parachutes.[26] Additionally, these investigators found that in the right conditions the drag of decelerating objects may reverse directions as a result of violent wake recontact, thus, becoming a pushing force in the manner shown in Fig. 1 and yielding $-5 < C(t) < +4$ (Refs. 23–25). Of course, the drag function is always equal to the value of the familiar drag coefficient, that is, $C(t) = \text{cons} = C_D^{\text{steady}}$, when $V(t)$ is constant for long periods of time.

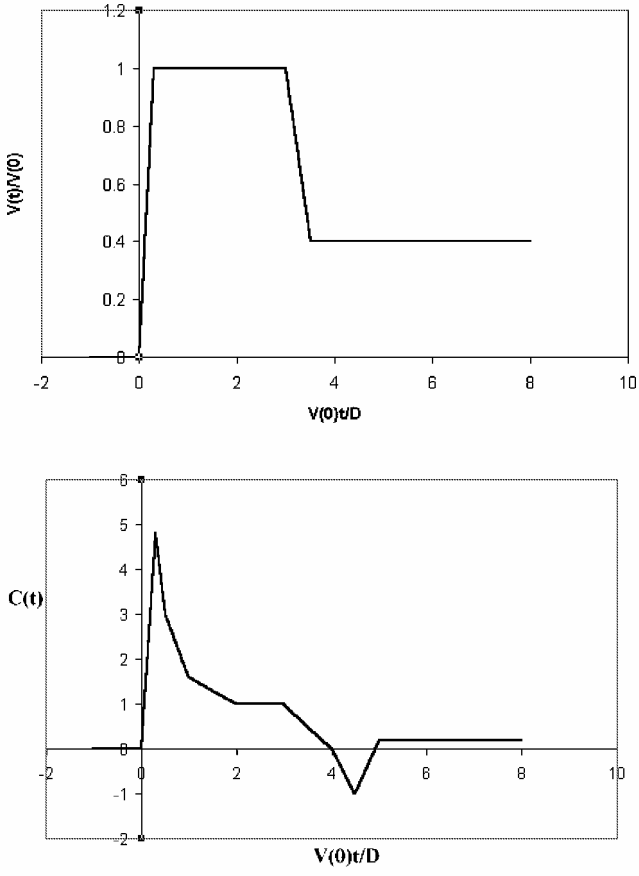

Fig. 1 Schematics of the speeds and drag functions characterizing disks moving in tow tanks.[23–25]

The mechanisms for such time dependence are many, as discussed, for example, by Sarpkaya and Isaacson[1] and by Sarpkaya.[2] Accelerated and decelerated motions imply a host of new phenomena caused by a changing Reynolds number, including time-dependent vortex shedding intervals and locations, hard to predict boundary-layer transitions, laminar-to-turbulent flow transitions and wake recontact. All of this has been documented by several tow tank studies of cylinders, plates and disks at low and medium Reynolds numbers (see Refs. 27–35) and in parachute test drops at high Reynolds numbers (see Refs. 17 and 26). Most important, such complexity makes it is very difficult to calculate from scratch the explicit time evolution of the drag function $C(t)$, given that it is not only specific to the trajectory studied and forces applied, but also to the history of the motion before being accelerated or decelerated. This is particularly true for decelerating motions, where fast-moving sections of wakes created before deceleration may be interacting again with the (now) slow-moving body moments after the onset of deceleration.

Several theoretical descriptions of decelerating body drag have been discussed in the past. These includes calculations using the concept of apparent mass,[1–20,36,37] the slug wake model of Spahr and Wolf,[38] the fluid–parachute interaction model of Oler,[39] and a generalization of Oler's model to include apparent mass by Yavuz and Oler.[40] Of note are also the numerical simulations of decelerating disks by Strickland[41] and their comparison with experimental data by Higuchi et al.,[23] Balligand and Higuchi,[24,25] and Higuchi and Strickland.[42] In the following we present an alternate model of decelerating bluff-body drag, which is not as general as Strickland's vortex computer simulations,[41] but is more reliable than the many models that use the added mass concept when separated flows are present. The model is also much simpler and is based on the following premises: first, that the wake of an object accelerating downwind in a moving fluid is identical to that of the same object decelerating in the fluid being at rest; second, that the drag force depends weakly on the instant deceleration $a(t)$ if the motion is characterized by a "low enough" acceleration modulus; and finally, that the drag force generated by a bluff body drifting freely with the wind at ground speed $V(t)$ and accelerating to the speed of the wind (V_{wind}) goes as $F_D \sim (V_{\text{wind}} - V)^{\beta}$. Using Galilean transformations to translate this result into deceleration drag provides the end result. Several trajectories can be studied with this formula, including the motion of a bluff body decelerating after moving in a state of acceleration, deceleration, or constant speed.

Equivalent Wakes for Decelerating and Accelerating Motions

Most relevant to the proposed model is the Galilean equivalence defined by a body decelerating in still air and the same body accelerating while drifting with moving air. Consider an object freely decelerating in static air under the influence of drag and a given external force, from an initial speed V_i to a final speed V_f . When observed from a reference frame moving along at a constant speed $V_{\text{ref}} > V_i$, this same object now appears to accelerate along with the air, which is now seen moving at constant speed of $V_{\text{wind}} = -V_{\text{ref}}$. The acceleration would be seen as generating speed changes from $V_i' = -V_{\text{wind}} + V_i$ to $V_f' = -V_{\text{wind}} + V_f$. Of course, the wake generated by the object must be fundamentally the same despite having different motions in each reference frame. This implies that an aeronaut in a balloon accelerating from a ground speed of $V_i' = 0$ ft/s to $V_f' = V_{\text{wind}} = 10$ ft/s while drifting in a 10 ft/s wind would experience a wake identical to that of the same balloon generated while decelerating in still air from $V_i = -10$ ft/s to $V_f = 0$ ft/s. Such a similarity can be mathematically expressed via the use of Galilean transformations.[43] These relate the coordinates, x, y, z, and t, speed V, and acceleration a of an object moving in one reference frame to the corresponding set of coordinates and variables of the same object seen from another reference frame moving at constant velocity V_{ref}. More specifically, these transformations are formulated as follows for a reference frame moving in the x direction:

$$x' = x - V_{\text{ref}}t, \qquad y' = y, \qquad z' = z, \qquad t' = t$$
$$V_x' = V_x - V_{\text{ref}}, \qquad a_x' = a_x \tag{2}$$

Note that by convention, all unprinted reference frames will correspond to frames where the fluid at infinity appears at rest, that is, there is no wind. These equations imply that the velocity components in the y and z directions, as well as the acceleration components in all three directions, remain invariant from one Galilean frame to another. Moreover, the acceleration being invariant means that the total force acting on the body is also invariant, as well as any individual force playing the role of the net force or combining with others into a net force. For example, in the case of a drag force and external force causing a one-dimensional motion,

$$F_{\text{tot}}' = F_{\text{tot}}, \qquad F_D' = F_D, \qquad F_{\text{ext}}' = F_{\text{ext}} \tag{3}$$

where

$$ma(t) = F_{\text{tot}} = -F_D + F_{\text{ext}} \tag{4}$$

Equations (1–4) can be used to write down the transformation properties of the drag function $C(t)$, to yield

$$C'(t')V'(t')^2 = C(t)V(t)^2 \tag{5}$$

This result means that the product CV^2 is a Galilean invariant. It also means that, when the unprimed reference frame is one where the fluid is at rest, the drag factor $C'(t)$ measured in the primed frame corresponds to a speed $V'(t)$ that is no longer equal to the speed of the moving body relative to the incoming air.

In discussions to follow, frequent use is made of the acceleration modulus, which is defined here in terms of the airspeed relative to the wake-producing object:

$$\delta = D|a| \big/ (V_{\text{rel}})^2 \tag{6}$$

Such definition ensures that it coincides with the definition[1,22] that is used in cases where the fluid is at rest. However, Eq. (6) also ensures that it is a Galilean invariant given that $\delta' = D|a'|/(V'_{\text{rel}})^2 = D|a|/(V_{\text{rel}})^2 = \delta$.

Trajectory Restrictions and Basic Assumptions

The proposed model is expected to be valid only within a specific set of initial and final conditions, as well as with specific trajectories and driving external forces. Fundamentally, one should always expect $C(t)$ to be very sensitive to initial conditions given that a decelerating body generates a wake that not only piles up on the backside of the body but also on itself. This means that wake sections produced at earlier times, in particular before deceleration, may strongly interact with the wake sections produced during deceleration.[38]

The model is defined for applications to bluff objects such as parachutes, which are decelerating from a high initial speed and high Reynolds number regime, that is, $Re \sim 10^5$–10^7, to a terminal velocity regime also characterized by a high Reynolds number. Moreover, the following conditions are assumed to hold.

1) External forces exhibit an asymptotic behavior of the type $F_{\text{ext}} \to Aa(t) + B$ as $t \to \infty$, where A and B are constants.

2) A body generates a turbulent wake, but one that is not necessarily fully developed, with the largest eddies being somewhat smaller than the size of the object producing the wake.

3) An acceleration modulus does not increase with time, but is initially nearly constant and later converges to zero as $t \to \infty$, as shown by the dashed curve of Fig. 2.

4) A value of the ratio of initial–to–final speeds (or V_i/V_f) is small enough to preclude the kind of wake recontact and drag reversal described in Refs. 23–26. For the types of geometrically porous parachute studied by Strickland and Macha,[26] this would amount to $V_i/V_f < 4$.

Requirement 1 ensures that the deceleration profile yields a speed converging to a constant value as the result of the applied forces combining into a null net force. Requirement 3 adds more restrictions on the type of trajectory, in particular eliminating from consideration most of the data generated in past tow tank experiments.[23–25,35] In general such experiments use a constant deceleration, which leads to an increasing acceleration modulus, in contrast to the decreasing acceleration modulus encountered with freely decelerating parachutes or drifting balloons (Fig. 2). Typically, and at similar initial decelerations and speeds, freely decelerating objects move faster than objects being towed at a fixed deceleration, thus generating less of a wake pile up. Thus, vastly different wakes and drag functions should be expected in both cases. Requirement 4 also eliminates all trajectories, freely decelerating[26] or decelerating in tow tanks,[23–25] that involve the reversal of the direction of the drag force[41,42] [where $C(t) < 0$]. This requirement arises from the mathematics of the model being too simplistic to handle correctly the effects of drag direction reversal [see subsequent Eq. (7)]. Finally, requirement 2 ensures that the body is moving at high values of Reynolds number where flow separation along its sides has already occurred. The drag generated under this requirement cannot always be described by formalisms based on the apparent mass concept.[3–20,36,37] A final requirement is as follows.

5) The value of $\delta(t)$ should not exceed an upper bound approximating 10^0.

This requirement is made to minimize (or eliminate) the explicit dependence of the drag function $C(t)$ on the deceleration $a(t)$, a most drastic approximation. This idea can be motivated by the piling up of the wake on the decelerating body and on itself, which leads to a partial washing-out (or averaging out) of the acceleration history contained in various portions of the wake. Such erasing action should be further enhanced by requirement 5, given that the high Reynolds number fluid flow around a decelerating disk is made up of ideal or potential flows enveloping the disk and its turbulent wake. Relative to the disk, such flows would be decelerating in a manner primarily determined by the deceleration evolution of the incoming flow, that is, $a(t)$. On the other hand, and at low enough $\delta(t)$, the rates of speeds of the fluid particles moving inside the near wake should be determined not by the instant value of $a(t)$, but rather by the high shear forces that are prevalent when the disk is moving near constant speeds. In fact, the accelerations of the near wake's fluid particles should be much greater than $a(t)$ in this regime.[44] Thus, having a large portion of the wake being weakly dependent on the instant value of $a(t)$ should lead to a drag function that is likewise dependent. A calculation using Prandtl's mixing length theory (see Ref. 45) can be used to estimate the required low value of the acceleration modulus.[44] Following the argument by Potvin[44] applied to the wakes of accelerating disks, one arrives at a bound of $\delta(t) < 10^0$. Note finally that assuming the drag function to depend weakly $a(t)$ also entails $C(t)$ being weakly dependent on the amount of external forces applied. This should be so as long as these forces do not directly perturb the flow about the body in any way other than by imparting different accelerations. In this respect, forces provided by thin ropes aligned with the incoming flow would satisfy this requirement, but propellers attached near the drag-producing features of a body would not.

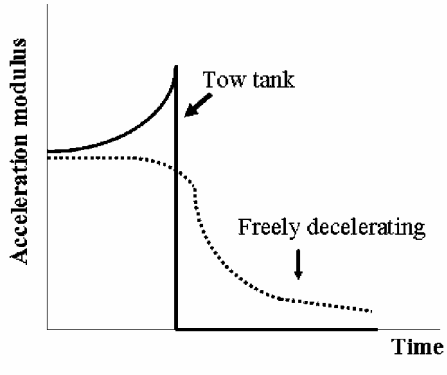

Fig. 2 Acceleration modulus comparison between motions studied in tow tank experiments and decelerations of freely moving vehicles.

From Wind Drifter Drag to Decelerating Parachute Drag

Drag Force of Wind Drifters

The equivalence between the wakes of wind drifters and of decelerating bodies in a static fluid will provide the starting point for the derivation of the model. First accelerating wind drifters sustaining no external force other than drag, that is, $F'_{\text{ext}} = 0$ in Eq. (4) are considered. The corresponding decelerator example would be that of a parachute (of the same shape) decelerating an unpowered vehicle/payload along the horizontal. Under such conditions, a wind drifter would settle in time into a constant speed that is equal to the speed of the wind. When a start from rest is considered, the drifter would start by accelerating with respect to the ground, all of the while generating a drag force decreasing in magnitude because of its decreasing speed relative to the wind. This process would continue until the drifter's ground speed becomes identical to that of the wind. At this point, the net force applied becomes zero, and the drifter proceeds at constant speed according to Newton's first law of motion. Thus, one obtains the following evolution, using Eq. (1) and (4), here expressed in terms of accelerations, speeds, and wind speeds measured with respect to the ground: $ma'(t) = -F'_D(t) \equiv -(\frac{1}{2})C'(t)\rho SV'(t)^2 \to 0$ as $t \to \infty$. Because $V' \to V'_{\text{wind}} \neq 0$, one would have $C'(t) \to 0$ as $t \to \infty$. Note that this limit would be valid regardless of drifter shape and speed range, but the specific manner in which this convergence occurs would be dependent on drifter shape and speed. For example, the limit would still apply for trajectories featuring drag reversal, but $\delta(t)$ and $C'(t)$ would not be monotonically decreasing.

Assuming no explicit dependence on $a(t)$ and no drag direction reversal permits the use of a very simple power law:

$$C(t)'V'^2 = B|V' - V'_{\text{wind}}|^\beta \tag{7}$$

where B and β are constants, to be later shown as dependent on initial conditions. This same power law will also be assumed to

hold in cases where $F'_{\text{ext}} \neq 0$, inasmuch as a weak dependence on the applied force has already been argued. In this case, the value of $C'V'^2_f$ would converge to a nonzero constant, where $C'(t) \to 2F'_{\text{ext}}/\rho S(V'_{\text{wind}} - V'_T)^2$, with the values of constants B and β being different from the freely drifting case, also as shown later. Finally, note that the initial condition $V'(0) = 0$ implies that $C'(0) = \infty$. This is not a real problem because a calculation or measurement of the drag force via Eq. (1) always involves first obtaining the value of the product $C'V'^2$, which by definition always remains finite. Thus, the drag function indeed diverges at $t = 0$ in this special case, but the drag force remains finite. This example points to the important fact that the drag function does not always have the interpretation normally attributed to the familiar drag coefficient. This is particularly true in reference frames where $V'(t)$ is not equal to the relative speed between the body and the incoming fluid.

Drag Force for Decelerating Motion in Static Fluids

The drag equation for a decelerating body identical in shape to that of the drifter discussed earlier can be derived by using Eq. (7) and the Galilean transformations (2–3). Looking at a wind drifter moving to the right from a reference frame also moving to the right but at wind speed $V'_{\text{ref}} = V'_{\text{wind}}$ shows the drifter decelerating in static air and to the left, from an initial speed $V_i = V'_i - V'_{\text{ref}}$ to a final speed $V_f = V'_T - V'_{\text{ref}}$. Here V'_T is the terminal speed generated by the external force F'_{ext} when the latter is balanced by drag. See Eq. (4) with primed speeds and accelerations. Using Eq. (7) in concert with the identity $C(t)V(t)^2 = C'(t)V'(t)^2$ yields

$$C(t) = B|V(t)|^{\beta-2} \tag{8}$$

The values of B and β are now determined using Eq. (8) for both initial and final values of the drag coefficient, namely, $C(t=0) \equiv C^{\text{init}} = BV_i^{\beta-2}$ and $C(t=\infty) = C_D^{\text{steady}} = BV_T^{\beta-2}$. This leads to

$$C(t) = C^{\text{init}}|V(t)/V_i|^{\beta-2} \tag{9}$$

where

$$\beta = 2 + \frac{\ell n\left(C^{\text{init}}/C_D^{\text{steady}}\right)}{\ell n(V_i/V_T)} \tag{10}$$

Note that $V_i > 0$ and $V_i > V_T$ to be consistent with the idea of a body experiencing a deceleration. Also note that the value of the exponent β depends on F_{ext} through Eq. (10) and that reference to fluid density and viscosity is made implicitly through C^{init} and V_T. In this model, C^{init} must be positive, otherwise $C(t)$ is negative, and the drag force is reversed for the entire deceleration.

Applications and Predictions

A very important aspect of this model is that exponent β changes also with the value of the drag function at the beginning of the deceleration, that is, C^{init}. At first this seems a major weakness because C^{init} cannot always be measured simply in an experimental setting.[26] However, it is shown here that C^{init} can actually be calculated or measured in a few but nevertheless very important cases that encompass a great number of nontrivial trajectories. It must be emphasized again that the strong dependence on the value of C^{init} is not an artifact of the model. It is rather a fundamental characteristic of decelerating body drag, where wake sections generated before deceleration reinteract with the body soon after the onset of deceleration.

Powered Vehicle with Parachute in Tow

Powered vehicles towing inflated parachutes or any other high-drag devices have the capability of accelerating or cruising at constant speed before t_i. Consider, first, the case where the vehicle is traveling at constant speed, namely, $V(t \le t_i) = V_i > V_T$, and at a high enough Reynolds number so that C_D^{steady} is nearly speed independent. The value of $C(t < t_i)$ representing the combined parachute drag and vehicle drag should be close to its steady-state value, namely, $C^{\text{init}} \sim C_D^{\text{steady}}$. According to Eqs. (9) and (10), this means that $\beta \sim 2$, to yield a constant value of the drag function and a drag force depending on speed as $F_D \propto V^2$.

Accelerating the vehicle before deceleration provides more interesting scenarios and will give many different drag force evolutions. This is demonstrated by using the accelerating disk drag evolution equations recently derived in Ref. 44. These formulas are based on the tow tank data of Iversen and Balent,[22] who studied the motion of submerged disks being pulled upward from rest, by a rope attached to weights falling outside the tank. These investigators showed that the resulting unsteady drag was strongly correlated with the acceleration modulus δ. Fitting their data with the appropriate logarithmic law yielded (where $C_D^{\text{steady}} \sim 1.1$)[44]:

$$C^{\text{disk}}(t) \approx C_D^{\text{steady}} \cdot (4.67)^{\delta(t)^{0.65}}, \qquad 0 < \delta < 0.3 \tag{11}$$

$$C^{\text{disk}}(t) \approx [20 \cdot \delta(t)]^{0.46}, \qquad 0.3 < \delta < 10 \tag{12}$$

$$C^{\text{disk}}(t) = C_D^{\text{steady}} + 2K(\nu_{\text{disk}}/SD)\delta(t), \qquad \delta \gg 10 \tag{13}$$

Equations (11) and (12) were defined to have the same value and the same slope at $\delta = 0.3$. This particular value of the acceleration modulus marks, in this particular experiment, a distinct but smooth transition between the high and low δ regimes.

Returning to the study of powered vehicles towing a parachute/disk device, equations (4) and (11–13) can be now used to calculate the value of C^{init} for a variety of acceleration profiles generated by constant traction or thruster forces. This is shown in Tables 1 and 2, which display the values of $\beta - 2$ and C^{init} for different initial conditions. In both acceleration and deceleration phases, the applied external force is constant at all times except at t_i (the beginning of the deceleration phase), where possibly $F_{\text{ext}}(t < t_i) \neq F_{\text{ext}}(t \ge t_i)$. Note that writing the initial value of the acceleration modulus as $\delta(t_i - \varepsilon) \equiv \delta_{t_i - \varepsilon}$ in Tables 1 and 2 reflects the fact that the value of δ just before the beginning of the deceleration may not be the same just after, given that our model may not yield a continuous $a(t)$ at $t = t_i$.

Some interesting estimates using the results of Tables 1 and 2 can be obtained by studying the example of an aircraft towing a deceleration parachute/disk where, before t_i, the aircraft provides (constant) thrust in much greater amounts than drag, thereby causing an acceleration. Engine power is then reduced at t_i to begin the deceleration phase. Assuming a modulus of $\delta(t_i - \varepsilon) \sim 0.5$ just before the deceleration phase would give a maximum drag coefficient of $C^{\text{init}} = 2.88$ according to Table 2. Being dependent on initial and final speed, exponent $\beta - 2$ would then be approximated by $\beta - 2 \sim 0.6$, 1.39, and 5.33 for speed ratios of $V_i/V_T \sim 5.0$, 2.0, and 1.20, respectively. In

Table 1 Values of exponent $\beta - 2$ for different initial conditions[a]

Accelerating disk, $t < t_i$	Value
$0 \le \delta \le 0.3$	$\dfrac{\delta_{t_i-\varepsilon}^{0.65}\,\ell n 4.67}{\ell n(V_i/V_T)}$
$0.3 \le \delta \le 10.0$	$\dfrac{\ell n\left[\left(20 \cdot \delta_{t_i-\varepsilon}\right)^{0.46}/C_D^{\text{steady}}\right]}{\ell n(V_i/V_T)}$
$\delta \gg 10.0$	$\dfrac{\ell n\left[1 + \left(2K\nu_{\text{disk}}\delta_{t_i-\varepsilon}/SDC_D^{\text{steady}}\right)\right]}{\ell n(V_i/V_T)}$

[a] $F_{\text{ext}}(t < t_i) \neq F_{\text{ext}}(t > t_i)$.

Table 2 Values of C^{init} for different initial conditions[a]

Accelerating disk, $t < t_i$	Value
$0 \le \delta \le 0.3$	$C_D^{\text{steady}} 4.67^{\delta_{t_i-\varepsilon}^{0.65}}$
$0.3 \le \delta \le 10.0$	$\left(20 \cdot \delta_{t_i-\varepsilon}\right)^{0.46}$
$\delta \gg 10.0$	$2K\nu_{\text{disk}}\delta_{t_i-\varepsilon}/SD$

[a] $F_{\text{ext}}(t < t_i) \neq F_{\text{ext}}(t > t_i)$.

other words, the drag force would vary as $F_D \propto V^{2.6}$, $V^{3.39}$ and $V^{7.33}$, respectively. Note that the drag force would go as $F_D(t) \propto V^2$ in the limit of very high V_i/V_T ratios, which implies constant $C(t)$ but one with a value different from C_D^{steady} (provided that there is no drag reversal).

Revisiting Freely Decelerating Body Dynamics

More interesting observations arise when revisiting the well-known solution of the freely decelerating body in a static fluid where F_{ext} is very small. In regimes where $V_i \gg V_T \neq 0$ and C_D^{steady} is V independent, one has $\beta \sim 2$ and

$$ma = -\tfrac{1}{2}C^{\text{init}}S\rho V^2 \tag{14}$$

a result that involves a constant drag coefficient in conformity with current practice. What is new here is that C^{init} may not be equal to the object's steady drag coefficient, as sometimes assumed, but determined by the motion's history before deceleration. Indeed, integrating Eq. (14) yields

$$V(t) = V_i\left[1 + \frac{V_i\rho SC^{\text{init}}}{2m}t\right]^{-1} \tag{15}$$

where, as expected, the speed would converge to zero in a timescale defined by the ratio $T_{\text{decel}} = 2m/V_i\rho SC^{\text{init}}$, as again determined by the motion's history. For example, assuming the object to have the profile of an accelerating disk in the range of $0.3 < \delta < 10$ before deceleration would imply a deceleration timescale of $T_{\text{decel}} = 2m/V_i\rho S[20\delta(t_i - \varepsilon)]^{0.46}$. Note also that Eq. (14) can be recast as follows, using Eq. (6):

$$\delta = \delta_i = \frac{C^{\text{init}}DS\rho}{2m} \tag{16}$$

This result underlines the little-known fact that the motion of a freely decelerating object is a motion of constant acceleration modulus. Like before, the value of δ would be determined by the motion's history as illustrated by case of the accelerated disk just studied: $\delta_i = [20 \cdot \delta(t_i - \varepsilon)]^{0.46}(DS\rho/2m)$.

Comparison with Parachute Drop Data

The experimental validation of the ideas embodied in Eqs. (9) and (10) is carried out using the data of parachute drops recently performed by the authors. Like disks, parachutes display no boundary-layer transitions because of airflow separation taking place at the leading edge, that is, skirt of the canopy.[46] Therefore, parachutes can be considered bluff in the same way disks are. Also, the low-speed character of the drops ensured that no drag reversal ever took place, given that the recontact of the wake of slow parachutes results only in small deformation of the crown. (Drag reversal occurs on parachutes and other flexible objects only after the entire body has suffered major deformations.) In the following, the proposed drag model is applied to the postinflation phase, where the canopy decelerates to terminal speed while remaining fully inflated.

Experimental Conditions

The specifics of the tests that generated the data are discussed in detail in Ref. 47. Briefly, these tests consisted in dropping low fabric permeability round parachutes and cruciform parachutes from aircraft flying at 1100 ft (335 m) mean sea level, at speeds ranging between 90- and 110-kt indicated airspeed. The parachutes carried suspended loads of 100 lb (445 N). The drag force sustained by the parachutes was measured using load cells inserted on each strap linking the parachute to the payload. (Such straps are called risers.) The parachute's rate of descent after inflation was measured by an electronic barograph also located on the payload. These instruments sent data to an onboard data acquisition system recording at a rate of 500 Hz.

The parachutes tested were as follows: A 15-ft-diam, half-scale model of the U.S. Air Force C-9 personnel emergency flat circular parachute and a 28-ft-diam (8.5-m) personnel emergency flat circular parachute used by the U.S. Navy. References 46–49 give ample details on their construction, including the type of cloth used. These parachutes were found to have a 22 ft/s (6.7 m/s) and 16.6 ft/s (5.0 m/s) terminal descent rate while carrying payloads of 100 and 120 lb (444.8 and 533.7 N), respectively. The other parachutes tested included a one-of-a-kind U.S. Army humanitarian cargo delivery cruciform parachute of 3–1 aspect ratio, built out of two 9.2 by 24.0 ft (2.8 by 7.3 m) panels sewn into a cross and attached to 20 suspension lines of length 19.7 ft (6.0 m). Also tested were (approximately) half-scale models of this U.S. Army cruciform parachute, built out of two 4.2 by 10.7 ft (1.3 by 3.3 m) panels and 20 suspension lines of length 12.2 and 17.0 ft (3.7 and 5.2 m). The terminal speed of these cross chutes was measured at 17.8 and 32 ft/s (5.4 and 9.7 m/s) while carrying payloads of 100 and 128 lb (444.8 and 569 N), respectively.

Initial Conditions and Inflation Model

Testing Eqs. (1), (9), and (10) during the postinflation phase requires using initial postinflation deceleration data, that is, V_i and C^{init}, which in turns requires the knowledge of the parachute's descent rate and drag function obtained at the very end of the inflation phase. This further requires the knowledge of the fall rate and drag function of the parachute during the entire inflation phase. As discussed in Ref. 26, directly calculating the drag factor from test drop data in general is particularly difficult given that the needed acceleration, instant opened surface area, and velocity evolutions have to be measured independently and at a level of accuracy that is beyond the capabilities of our instrumentation package. Instead, we have used a well-established simulation method to duplicate the time dependence of the parachute riser force, drag area, and payload descent rate during inflation.[46,50] The formalism is based on the use of the following equations of motion, written here to simulate the tangential deceleration and speed along the ballistic-like trajectory of a payload–parachute system dropped from aircraft[13,50]:

$$ma = -\frac{1}{2}\rho S(t)C(t)V^2 + W\cos\theta \tag{17}$$

$$S(t)C(t) = b_1 t^6 + b_0 \tag{18}$$

$$\frac{\mathrm{d}\theta}{\mathrm{d}t} = -g\frac{\sin\theta}{|V|} \tag{19}$$

The constant b_0 corresponds to the parachute's drag area before inflation, that is, $b_0 = S(0)C(0)$. On the other hand, b_1 is expressed in terms of b_0 and of the drag area at the end of the inflation phase, namely, as $b_1 = [(S(t_f^{\text{infl}})C(t_f^{\text{infl}}) - b_0)]/(t_f^{\text{infl}})^6$. Test drops performed over the past decades have shown the t^6 law to work very well with most inflating, low permeability, and low geometric porosity parachutes such as cupped parachutes and low aspect ratio cruciform parachutes.[46] Established from the direct measurement of the ratio $2(ma - W\cos\theta)/\rho V^2$, this law takes into consideration all effects relevant to the unsteady aerodynamics acting on an inflating parachute, including coaccelerated air mass and the actual opening and spreading of the canopy. Note that Eq. (17) neglects the elastic response of the suspension lines and parachute cloth during inflation, which for the light payload weight used here allowed the full transmission of the drag force to the load measuring instrumentation in a timescale much shorter than the inflation time.

A comparison between the numerical solutions of Eqs. (17–19) and the measured riser loading during inflation is shown in Figs. 3–6. The computer simulations were carried out using the following sources of data for input parameter determination: direct measurements for m and ρ, video analysis for $S(0)$ and t_f^{infl}, load cell measurements for $F_{\text{drag}}(t)$, and rate of descent (terminal regime) for C_D^{steady}. Assuming $C(0) \sim 1$ to account for the drag of the payload box at the onset of inflation, and using $S(0)$ from video, gives the value of b_0 required by Eq. (18). On the other hand, the determination of b_1 required knowing not only the value of $S(t_f^{\text{infl}})$ and t_f^{infl} (obtained from video) but also the value of the product $S(t_f^{\text{infl}})C(t_f^{\text{infl}})$. This number, as well as the value of $V(0)$, was obtained by repeated

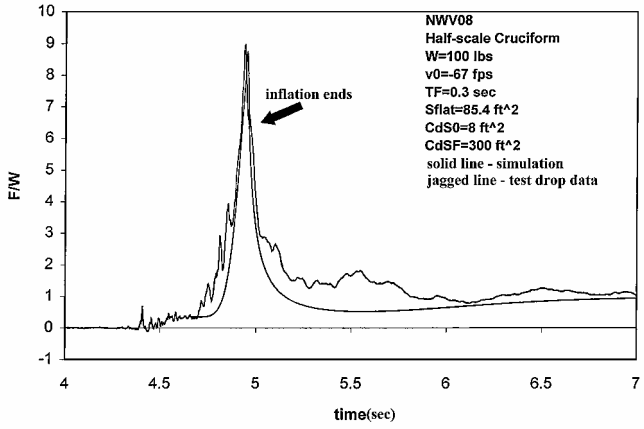

Fig. 3 Total parachute riser force per unit payload weight vs time.

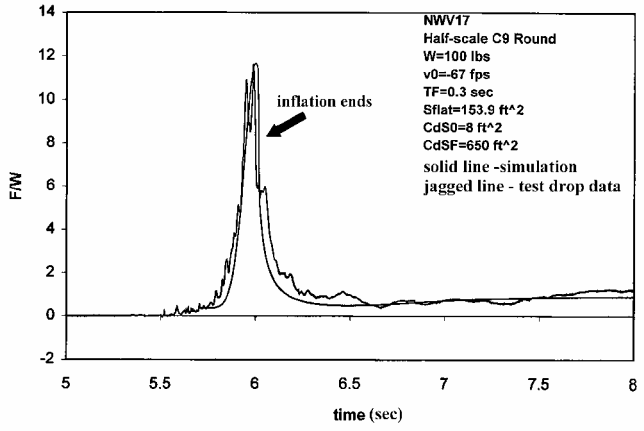

Fig. 4 Total parachute riser force per unit payload weight vs time.

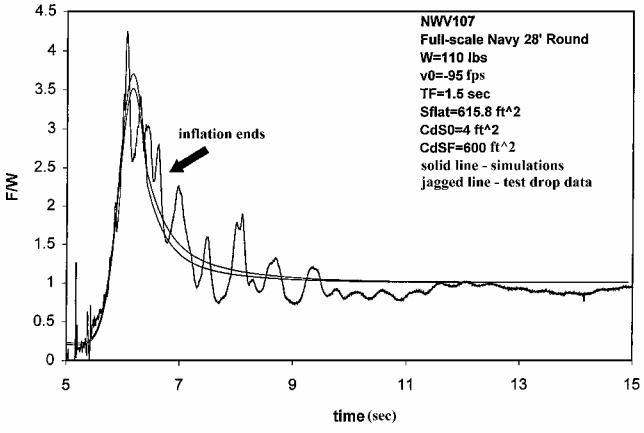

Fig. 5 Total parachute riser force per unit payload weight vs time.

simulations of Eqs. (17–19), until the best fit of the measured riser force was achieved, as shown in Fig. 7. (Some very good fits were achieved.)The values of all parameter used are shown in the figures.

Postinflation Deceleration and Drag Model Validation

During the postinflation phase, the equation of motion along the trajectory tangent evolves into the following form, which directly follows from Eqs. (1), (9), and (10):

$$ma = -\tfrac{1}{2}\rho S C^{\text{init}} (V/V_i)^{\beta-2} V^2 - \rho v_{\text{chute}}\, a + W\cos\theta \qquad (20)$$

Here the time dependence of the parabolic trajectory angle is still, given by Eq. (19). Note that the value of β, V_i, and C^{init} required for the solution of Eq. (19) and (20) are completely determined by the ending conditions of the inflation phase simulation. No further

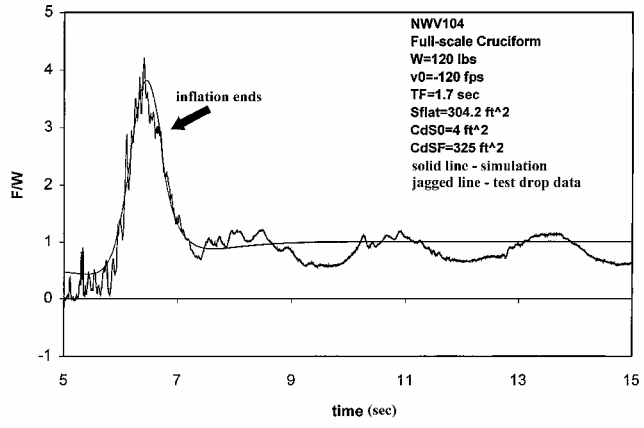

Fig. 6 Total parachute riser force per unit payload weight vs time.

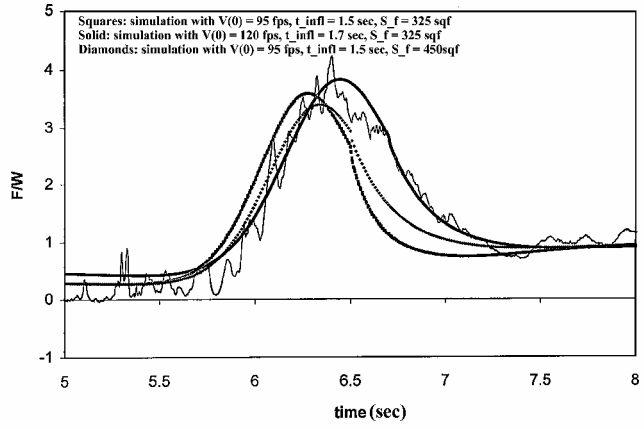

Fig. 7 Riser loads vs time; same drop and parachute construction data as in Fig. 6.

tuning of the drag model is actually possible. Figure 7 shows that the model performs well when the inflation simulation performs well and performs badly when the former performs badly. The comparison between theory and experiment is also shown in Figs. 3–6.

Comparison with Experiment

Figures 3–6 show the comparison between the calculated and experimental riser force, during and after inflation. In agreement with most unreefed parachutes studies of the past,[46] the computer simulations show the moment of maximum opening force to occur before the full spreading of the parachute. When the small-amplitude fluctuations in measured drag caused by the elastic nature of the suspension lines and fabric flutter (and possibly by local wake recontact effects) are discarded, the agreement between theory and experiment is good for both cruciform parachute sizes and for the half-scale round parachute (C-9 parachute). For these cases, our deceleration model gives a good estimate of the deceleration rates after the end of inflation (very high rates) and just before settling into terminal velocity (very low rates). According to Eq. (9), such rates should be proportional to $V^{\beta-1}$. On the other hand, the match between theory and experiment for the full-scale Navy round parachute example could be best characterized as "fair," for reasons to be discussed further.

Figures 8–11 show the corresponding time evolution of the calculated drag coefficient. Figure 10 in particular shows the effect of changing the values of V_0 and $C(t_f^{\text{infl}})S_f$. Quite remarkably, the half-scale parachutes feature higher values and rates than the full-scale parachutes. This is explained by that both sizes of parachutes were deployed at the same speed and altitude, thereby causing the inflation time scale to become much smaller for the half-scale than for the full-scale parachutes, that is, twice as fast for the half-scale parachutes.[46] Not having the time to decelerate substantially causes

Table 3 Calculated deceleration properties of the parachutes studied in the test drops[a]

Property	Half-scale cross $D = 10.7$ ft	Half-scale C-9 $D = 15.0$ ft	Full-scale cross $D = 24.0$ ft	Full-scale U.S. Navy $D = 28.0$ ft
$C^{\text{init}}/C_D^{\text{steady}}$	3.25	3.12	1.06	≈ 1.00
V_i/V_T	1.43	1.33	1.63	1.52 and 1.41
β	5.29	5.98	2.12	1.95 and 2.13
$\delta(t_i)$	0.64	2.31	1.24	3.17

[a]Input data shown in Figs. 3–6.

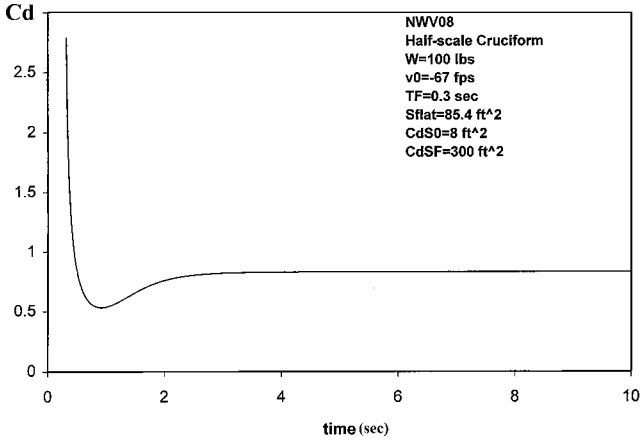

Fig. 8 Calculated drag coefficient vs time during the postinflation deceleration phase; same input parameters as in Fig. 3.

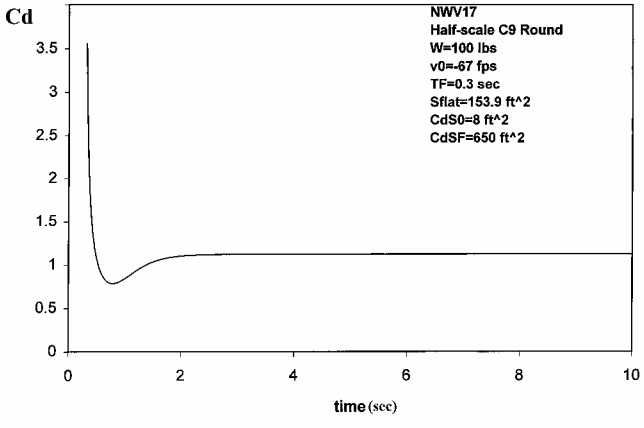

Fig. 9 Calculated drag coefficient vs time during the postinflation deceleration phase; same input parameters as in Fig. 4.

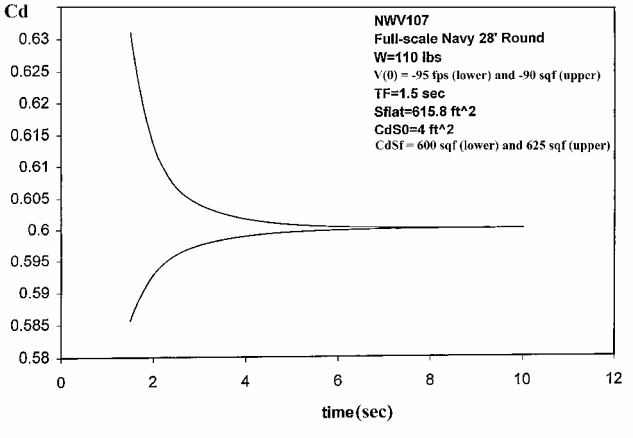

Fig. 10 Calculated drag coefficient vs time during the postinflation deceleration phase; same input parameters as in Fig. 5.

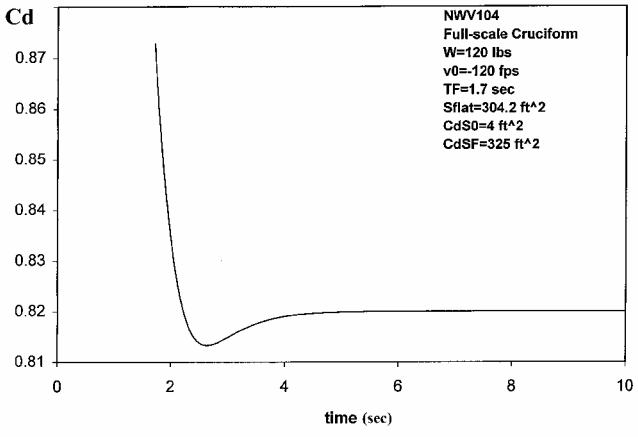

Fig. 11 Calculated drag coefficient vs time during the postinflation deceleration phase; same input parameters as in Fig. 6.

the smaller chutes to open at higher $V(t)$, leading to quicker openings and higher forces than the larger chutes. All of this would contribute to drag coefficients that would be larger for the former than for the latter. Table 3 shows the calculated values of $C^{\text{init}}/C_D^{\text{steady}}$ and β for the four parachutes tested. According to Eq. (10), the drag force would vary as $F_D \propto V^{5.29}$, $V^{5.98}$, $V^{2.12}$, and $V^{2.00}$ for the half-scale cruciform parachute, half-scale C-9 parachute, full-scale cruciform parachute, and the full-scale U.S. Navy round parachute, respectively.

With regard to the trajectory requirements discussed earlier, Table 3 also shows the values of the ratio V_i/V_f as calculated from the numerical solutions of the model. Averaged at $V_i/V_f \sim 1.5$, these values fall well below the limit of $V_i/V_f < 4$ set forth by Strickland and Macha to avoid substantial canopy deformation/deflation from wake recontact.[26] Table 3 also shows the simulated values of the deceleration modulus at the beginning of the postinflation phase, pointing to all drops being in the desired range of $\delta_{\text{init}} \sim 10^0$, namely, $\delta_{\text{init}} \leq 3.0$. In that respect, looking again at Figs. 3–6 shows that the agreement with experiment is actually better for those cases where $\delta_{\text{init}} \sim 1$ or less.

Conclusions

A new model of the drag force generated by a decelerating bluff body was derived and shown to compare favorably with parachute deceleration data collected during recent test drops. Its most interesting features are as follows: 1) a clear dependence on the history of the trajectory before deceleration; a nontrivial speed-dependence of the drag force, translating into power laws that are much different from the familiar V^2 power law; 3) an illustration of the deep connection between decelerating parachute aerodynamics and accelerating wind drifter aerodynamics; and 4) a great number of interesting applications, including the motions of inflated parachutes and the motions of disk-like shapes that accelerate and decelerate sequentially.

Further comparison with experimental data is of course necessary. Most useful would be the data of a tow-tank experiment similar to that of Higuchi et al.[23] and Balligand and Higuchi,[24] but dedicated to the study of constant decelerating motions without drag direction reversal (if such a correlation is possible). It would help clarify

whether Eqs. (9) and (10) can be used for decelerations that yield an increasing and discontinuous $\delta(t)$. Comparison with computational fluid dynamics-type computer simulations such as Strickland's[41] should be entertained as well. Combining the predictions of the model with the results of the latter would be very useful in assessing quantitatively the effects of various initial motions before deceleration.

Acknowledgments

This work was supported by the U.S. Army Soldier, Biological and Chemical Command (SBCCOM) under Contract DAAD16-00-C-9250 and by the U.S. Air Force Office of Scientific Research (AFOSR) under Grant F49620-98-1-0125. The authors thank R. Benney, C. Lee, and S. Patel (SBCCOM–Natick, Massachusetts) and S. Walker (AFOSR) for their advice and support. We also thank J. T. Blimling, R. Kutz, R. Eddy, J. Gentry, O. Guerrero, C. Loehner, C. Manglano, J. Mark, J. Papke, T. Perschbacher, G. Poston, T. Poston, and B. Yavitz for their help during the experimental phase of the project. J. Potvin also thanks W. Thacker and K.-F. Doherr for many fruitful discussions.

References

[1]Sarpkaya, T., and Isaacson, M., *Mechanics of Wave Forces on Offshore Structures*, Van Nostrand Reinhold, New York, 1981, pp. 52–149.

[2]Sarpkaya, T., "Method of Analysis for Flow Around Parachute Canopies," 11th *AIAA Aerodynamic Decelerator Systems Technology Conference*, AIAA Paper 91-0825, AIAA, Washington, DC, 1991, pp. 1–17.

[3]Cockrell, D. J., and Haidar, N. I. A., "Influence of the Canopy-Payload Coupling on the Dynamic Stability in Pitch of a Parachute System," AIAA Paper 93-1248, May 1993.

[4]White, F. M., and Wolf D. F., "A Theory of Three-Dimensional Parachute Dynamic Stability," *Journal of Aircraft*, Vol. 5, No. 1, 1968, pp. 86–92.

[5]Doherr, K.-F., "Theoretical and Experimental Investigation of Parachute-Load-System Dynamic Stability," AIAA Paper 75-1397, 1975.

[6]Tory, C., and Ayres, R., "Computer Model of a Fully Deployed Parachute," *Journal of Aircraft*, Vol. 14, 1977, pp. 675–679.

[7]Eaton, J. A., and Cockrell, D. J., "The Validity of the Leicester Computer Model for a Parachute with Fully-Deployed Canopy," AIAA Paper 79-0460, March 1979.

[8]Yavuz, T., and Cockrell, D. J., "Experimental Determination of Parachute Apparent Mass and its Significance in Predicting Dynamic Stability," AIAA Paper 81-1920, Oct. 1981.

[9]Cockrell, D. J., and Doherr, K.-F., "Preliminary Considerations of Parameter Identification Analysis from Parachute Aerodynamic Flight Test Data," AIAA Paper 81-1940, Oct. 1981.

[10]Doherr, K.-F., and Saliaris, C., "On the Influence of Stochastic and Acceleration Dependent Aerodynamic Forces on the Dynamic Stability of Parachutes," AIAA Paper 81-1941, 1981.

[11]Eaton, J. A. "Added Mass and the Dynamic Stability of Parachutes," *Journal of Aircraft*, Vol. 19, 1982, pp. 414–416.

[12]Heinrich, H. G., and Haak, E. L., "Stability and Drag of Parachutes with Varying Effective Porosity," Rept. ASD-TDR-62-100, Wright–Patterson AFB, OH, Sept. 1962.

[13]Lingard, J. S., "The Effects of Added Mass on Parachute Inflation Force Coefficients," *13th AIAA Aerodynamic Decelerator Systems Technology Conference*, AIAA Paper 95-1561, AIAA, Washington, DC, 1995, pp. 176–185.

[14]Lissaman, P. B. S., and Brown, G., "Apparent Mass Effects on Parafoil Dynamics," *12th RaeS/AIAA Aerodynamic Decelerator Systems Technology Conference*, AIAA Paper 93-1236, Washingtom, DC, 1993, pp. 233–239.

[15]Brown, G. J., "Parafoil Steady Turn Response to Control Input," *12th RaeS/AIAA Aerodynamic Decelerator Systems Technology Conference*, AIAA Paper 93-1236, Washingtom, DC, 1993, pp. 248–254.

[16]Ibrahim, S. K., "Apparent Added Mass and Moment of Inertia of Cup-Shaped Bodies in Unsteady Incompressible Flow," Ph.D. Dissertation, Univ. of Minnesota, 1965.

[17]Cochran, B. C., White, B. R., and Macha, J. M., "Experimental Investigation of Added Mass During Parachute Deceleration: Preliminary Results," AIAA Paper 91-0853, Washingtom, DC, pp. 171–180.

[18]Macha, J. M., "Simple Approximate Model of Parachute Inflation," *12th RaeS/AIAA Aerodynamic Decelerator Systems Technology Conference and Seminar*, AIAA Paper 93-1206, Washingtom, DC, 1993, pp. 44–53.

[19]Wolf, D. E., "Simplified Dynamic Model of Parachute Inflation," *Journal of Aircraft*, Vol. 11, No. 1, 1974, pp. 28–33.

[20]McVey, D. F., and Wolf, D. E., "Analysis of Deployment and Inflation of Large Ribbon Parachutes," *Journal of Aircraft*, Vol. 11, No. 1, 1974, pp. 96–103.

[21]Blevins, R. D., *Applied Fluid Dynamics Handbook*, Krieger, Malabar, FL, 1992.

[22]Iversen, H. W., and Balent, R., "A Correlating Modulus for Fluid Resistance in Accelerated Motions," *Journal of Applied Physics*, Vol. 22, 1951, pp. 324–328.

[23]Higuchi, H., Balligand, H., and Strickland, J. H., "Numerical and Experimental Investigations of the Flow Over a Disk Undergoing Unsteady Motion," *Journal of Fluids and Structures*, Vol. 10, 1996, pp. 705–719.

[24]Balligand, H., and Higuchi, H., "Wake of a Decelerating Disk," *12th RaeS/AIAA Aerodynamic Decelerator Systems Technology Conference and Seminar*, AIAA Paper 93-1218, Washingtom, DC, 1993, pp. 147–156.

[25]Balligand, H., and Higuchi, H., "Experimental Investigation of the Wake Behind a Solid Disk," Sandia National Labs., Rept SAND90-7083, Dec. 1993.

[26]Strickland, J. H., and Macha, M., "Preliminary Characterization of Parachute Wake Recontact," *Journal of Aircraft*, Vol. 27, No. 6, 1990, pp. 501–506.

[27]Keim, S. R., "Fluid Resistance to Cylinders in Accelerated Motions," *Journal of Hydraulic Division, ASCE*, Vol. 82, No. HY6, 1956, pp. 1113-1–1113-14.

[28]Stelson, T. E., and Mavis, F. T., "Virtual Mass and Acceleration in Fluids," *Proceedings of the ASCE*, Vol. 81, Separate No. 670, 1955, pp. 670-1–670-9.

[29]Laird, A. D. K., and Johnson, C. A., "Drag Forces on Accelerated Cylinders," *Journal of Petrolium Technology*, Vol. 8, 1956, pp. 56–67.

[30]Laird, A. D. K., Johnson, C. A., and Walker, R. W., "Water Forces on Accelerated Cylinders," *Journal of Waterways and Harbor Division, ASCE*, No. WW1, 1959 pp. 99–119.

[31]Sarpkaya, T., and Garrison, C. J., "Vortex Formation and Resistance in Unsteady Flow," *Journal of Applied Mechanics*, Vol. 30, Ser. E, 1963, pp. 16–24.

[32]Odar, F., and Hamilton, W. S., "Forces on a Sphere Accelerating in a Viscous Fluid," *Journal of Fluid Mechanics*, Vol. 18, 1964, pp. 302–314.

[33]Mavis, F. T., "Virtual Mass of Plates and Discs in Water," *Journal Hydraulics Division, ASCE*, 1970, 1947–1952.

[34]Hamilton, W. S., and Lindell, J. E., "Fluid Force Analysis and Accelerating Sphere Tests," *Journal of Hydraulic Division, ASCE*, Vol. 97, No. HY6, 1971, pp. 805–817.

[35]Tatsuno, M., and Taneda, S., "Visualization of the Unsteady Flow Past Cylinders and Plates Decelerating from a Steady Speed," *Journal of the Physical Society of Japan*, Vol. 31, 1971, pp. 1266–1274.

[36]Lamb, H., "On the Motion of Solids Through a Liquid," *Hydrodynamics*, 6th ed., Dover, New York, 1945, pp. 160–201.

[37]Thomasson, P. G., "Equations of Motion of a Vehicle in a Moving Fluid," *Journal of Aircraft*, Vol. 37, No. 4, 2000, pp. 630–639.

[38]Spahr, H. R., and Wolf, D. F., "Theoretical Analysis of Wake-induced Parachute Collapse," AIAA Paper 81-1922, Oct. 1981.

[39]Oler, J. W., "Prediction of Parachute Collapse Due to Wake Recontact," AIAA Paper 89-0901, April 1989.

[40]Yavuz, T., and Oler, J. W., "Theoretical Modeling of Wake-Recontact for a Parachute System," AIAA Paper 93-1219, May 1993.

[41]Strickland, J. H., "Prediction Method for Unsteady Axisymmetric Flow over Parachutes," *Journal of Aircraft*, Vol. 31, 1994, pp. 637–643.

[42]Strickland, J. H., and Higuchi, H., "Parachute Aerodynamics: an Assessment of Prediction Capability," *Journal of Aircraft*, Vol. 31, 1995, pp. 241–252.

[43]French, A. P., *Newtonian Mechanics*, MIT Introductory Physics Series, Norton, New York, 1971, pp. 173–178.

[44]Potvin, J., "Accelerating Disk Drag: Theory and Applications," AIAA Paper 2002-3055, June 2002.

[45]Schlichting, H., *Boundary Layer Theory*, 7th ed., McGraw–Hill, New York, 1987, Chap. 24.

[46]Knacke, T. W., *Parachute Recovery Systems Design Manual*, Para, Santa Barbara, CA, 1992.

[47]Potvin, J., Peek, G., Brocato, B., Kutz, R., and Yavitz, B., "Deceleration Dynamics of Unreefed Cruciform and Flat Circular Parachutes During and After Inflation," AIAA Paper 2001-2028, May 2001.

[48]Lee, C. K., "Model of Parachute Opening: An Experimental Investigation," *Journal of Aircraft*, Vol. 26, No. 5, 1989, pp. 444–451.

[49]Lee, C. K., "Experimental Investigation of Full-Scale and Model Parachute Opening," *8th AIAA Aerodynamic Decelerator Systems Technology Conference*, AIAA Paper 84-0820, AIAA, New York, 1984, pp. 215–223.

[50]Ludtke, W. P., "Technique for the Calculation of the Opening-Shock Forces for Several Types of Solid Cloth Parachutes," 4th *AIAA Aerodynamic Decelerator Systems Technology Conference*, AIAA, New York, 1973, pp. 176–185.